Curvelet Transformed Medical Image Fusion through Regional Entropy Distribution Characteristics

Xiaojun Wang, Yaru Zhu
Science & Technology College
North China Electric Power University
Baoding 071051
HeBei Province, P. R. China

ABSTRACT: *Multi-modal digital medical image fusion has drawn extensive attentions for integrating more information into one image. In this article, novel multi-resolution curvelet entropy distribution method is proposed to discriminate the image curvelet-transformed coefficients. Fusion weight determination for individual source information has been emphasized on, which is represented through analyzing the coefficient matrix in curvelet-transformed scale. Shannon entropy has been applied as the essential fusion weight criteria after counting the probabilities of the coefficients through different-sized masks at every scale. Fusion criterion of entropy distribution variance in different sized neighborhood regions is also combined with the entropy idea to preserve more details of the source images. After operating fusion on brain CT/MRI data sets, quantitative evaluation shows that the proposed approach based on 3×3 regional distribution of 3×3 masked entropy can provide more satisfactory fusion effect. And the wider mask or region can sensitively extract more CT information for fusion, though deteriorated the total fusion quality. The proposed algorithm is beneficial for multi-modal medical image comprehension to heighten the clinical diagnosis accuracy.*

Keywords: Image Fusion, Curvelet Transform, Entropy Distribution, Ridgelet Transform, Medical Image Processing

Received: 18 March 2019, Revised 9 June 2019, Accepted 22 June 2019

DOI: 10.6025/jmpt/2019/10/3/87-103

1. Introduction

Medical images have played more and more important roles during clinic diagnostics, which can be acquired by the radiological techniques based on X-ray, γ-emission, nuclear magnetic resonance, or even ultrasonic in some extents [1-2]. Variant responses can be initiated by radiological scan on different human inner organs, and then image is generated between such response contrasts. For example, the two-dimensional (2-D) image of skeleton can be obtained by different X-ray transmission character through skeletal or muscular structure [3]. In order to achieve higher image resolution and greater clinical accuracy, computer-aided medical image processing has been widely applied. One of the development trends is to simulate the real biological organ structure, and digital geometry processing is used to generate three-dimensional (3-D) image of the inner organ structure based

on the same imaging modality as a large slice of 2-D images [4-5]. The other trend is about clinical information extraction from multiple modal images including CT (computerized tomography), MRI (magnetic resonance imaging), PET (positron emission tomography), SPECT (single-photon emission computed tomography), US(ultrasonic) etc., with algorithms developed for image denoising, enhancement, edge detection, feature recognition, and so on [6-10].

When it comes to the multi-resourced images used for the above stated applications, the images are usually obtained from respective instruments, even though multi-modal radiology instrument has attracted industrial notices and several kinds of expensive multi-modal instruments recently been pushed out to market [11]. Image fusion of such multi-resource signals is the basic procedure not only for 3-D image establishing but also for clinical joint-information analyzing. The digital data sets or coefficient matrices mapped from multi-resource images are treated with mathematical and statistical methods for combining different-resource characteristics into one image, and can be processed in three levels including pixel level, feature level and decision level [12-14]. Fusing medical image in pixel level can provide increasing interpretation capabilities and reliable results, and has drawn extensive attentions from research to practical application viewpoints [15].

The pixel level fusion is involved with the information mining and statistical weight factor decision from different resource digital image data sets. The features of coefficient matrix mapped from image can be extracted for fusion weight classification based on the well-known algorithms such as intensity-hue-saturation (IHS) [16], SVMs (support vector machines) [17], neural network (NN) [18] and so on. Just as *Fourier* transformation generating frequency-scale information from time-scale signal, multi-resolution analysis plays important role in image processing. The 2-D digital matrix of image can be decomposed into small components from the coarse to fine scales, and then image fusion is operated in multi-resolution scales [19-20]. *Bhatnagar* et al. establish two algorithms based on visibility measure or texture information derived from framelet transform, and applied on MRI/CT and MRI/PET data matrices to maximally utilize the different modal information in low-frequency and high-frequency sub-bands [21]. Wavelet transformation modulus maxima can be applied to fuse multi-modal medical images by determining the essential coefficients [22]. *Shah* et al. propose fusion rules for CT and MRI images based on multi-resolution decomposition of the source images using wavelet, wavelet-packet, and contourlet transform, and then the weighted average factor of the source pixels is given based on the corresponding children pixels in the finer resolution bands. [23]. *Lewis* et al. report a novel region-based image fusion method through calculating each region characteristics in the wavelet domain [24]. Many reports have proposed wavelet-based algorithms for medical image fusion [25-28].

Though wavelet is acted as optimal tool for analyzing 1-D piecewise smooth signals, it has serious limitations when dealing with high dimensional signals such as images, and can only capture limited directional information, whereas image features usually occur along curves or edges in two-dimension or even three-dimension [29]. Other than wavelet transform, recently proposed curvelet method is a candidate for higher dimensional transformation to represent images at different scales and different angles. In 2006, *E. Candès* et al. describe the most cited second generation curvelet transform method in two and three dimensions, based on the fast wrapping on special *Fourier* samples. Digital images are represented by digital curvelet coefficients indexed by three parameters as scale, orientation and spatial location [30]. Curvelet transformation method is also focused on the fusion weight factor of the corresponding coefficients in the same scale from different images. *Li* et al. report that the multi-focus image fusion through the wavelet transformed fusing method to merge the curvelet transformed coefficients from individual source images in order to achieve better performance [31]. Low-pass and high-pass curvelet decomposed sub-bands can be manipulated by different fusion rules, such as the feature similarity (FSIM) or the complex coefficients feature similarity (CCFSIM) proposed by *Xu* et al. [32] *Sapkal* et al. enumerate several discrete curvelet transform fusion rules on multi-modal medical images, such as the minimum selection rule, PCA based rule, averaging rule, and so on [33].

In conclusion, image fusion is processed according to the statistically analysis in order to determine the significance of certain transformed coefficient in given scales. The more information embedded in a coefficient at a given resolution scale, the higher the significance of such coefficient becomes for further fusion. From the viewpoint of information theory, entropy is an adequate conception for measuring the uncertainty in a random variable, and usually refers to the *Shannon* entropy which quantifies the value of the information contained in a message [34]. In such means, the entropy and its 2-D regional distribution idea is put forward in this article as criterion to determine the fusion weights of coefficients in corresponding scale from different images. Neighborhood region distribution of the entropy is applied to preserve more details of the source images. Fusion experiments are operated on brain CT/MRI image data sets, and quantitative evaluation parameters such as image pixel entropy, average gradient, standard deviation and mutual information are applied to assess the fusion effect.

Purpose of this article is to put forwards a regional entropy distribution method in curvelet multi-resolution transform scale for

multi-modal medical image fusion. After briefly reviewing the ridgelet and curvelet transform methods in Section 2, the other sections of this article are arranged as follows. The fusion criterions are proposed in Section 3. In Section 4, such curvelet transform entropy distribution method is utilized for CT and MRI medical image fusion, and the quantitative evaluation on fusion performance is also present. Section 5 concludes the regional entropy distribution fusion method.

2. Curvelet Transformation Method

Curvelet transform displays great directional sensitivity and anisotropic advantages, which is adequate to decompose 2-D image into high resolution scales. The idea is to first decompose the image into a set of wavelet bands, and then analyze each band by ridgelet transform.

2.1. Ridgelet Transform

A basic strategy for calculating the continuous ridgelet transform on a signal f is firstly to compute the *Radon* transform $R_f(\theta, t)$ and secondly to apply a one-dimensional wavelet transform on the slices $R_f(\theta)$. The continuous ridgelet transform (*CRT*) coefficients in 2-Dimentional scale can be calculated as follows [30]:

$$CRT_f(a, b, \theta) = \int_{R^2} \psi_{a, b, \theta}(x) f(x) dx \tag{1}$$

where the ridgelet $\psi_{a, b, \theta}(x)$ is derived from wavelet-type function as

$$\psi_{a, b, \theta}(x) = a^{1/2} \psi\left(\frac{x_1 cos\ \theta + x_2 sin\ \theta - b}{a} \right) \tag{2}$$

To calculate the ridgelet coefficients, ridgelet analysis is operated in *Radon* domain. The *Radon* transform for an object function f is the collection of line integrals indexed by $(\theta, t) \in [0, 2\pi] \times R$ and is given as

$$R_f(\theta, t) = \int f(x_1, x_2)\, \delta(x_1 cos\ \theta + x_2 sin\ \theta - b)\, dx_1 dx_2 \tag{3}$$

with δ as *Dirac* distribution. The ridgelet transform can be represented as follows.

$$R_f(a, b, \theta) = \int_{-\infty}^{+\infty} R_f(\theta, t) a^{-1/2} \psi\left(\frac{t - b}{a} \right) dt \tag{4}$$

In Eq.(4), the ridgelet transform is the application of the 1-D wavelet transform to the slices of the *Radon* transform, where the angular variable θ is constant and t is varying component. To make the ridgelet transform into discrete, both the *Radon* transform and the wavelet transform should be set into discrete forms.

2.2. Curvelet Transform

The idea of curvelet is to represent a curve as a superposition of functions with various lengths and widths. This can be done by first decomposing the image into sub-bands, i.e. separating the object into a series of disjoint scales. Each scale is then analyzed by means of a local ridgelet transform [35]. Four procedures are carried out.

(1) Subband Decomposition

The sub-band decomposition is simply applying by convolution operator as $P_0 f = \Phi_0 * f$ and $\Delta_s f = \psi_{2s} * f$. Then the image is decomposed into sub-bands with the form of $f \rightarrow (P_0 f, \Delta_1 f, \Delta_2 f, \ldots)$. Each subband layer contains details in different frequency scale, with P_0 as low-pass filter dealing with low frequencies near $|\xi| \leq 1$, and Δ_s $(s = 1, 2, 3\ldots)$ as band-pass filters corresponding to frequencies near domains of $|\xi| \in 2^{2s}, 2^{2s+2}$. Such decomposition has the property of energy preservation as $\|f\|^2 = \| P_0 f \|^2 + \sum_s \|\Delta_s f\|^2$. For the two kind of components in low or high frequency domains, the $P_0 f$ can be efficiently represented using wavelet base as smooth (low-pass) section, and the discontinuity curves in the high-pass layers $\Delta_s f$ should be dissected into small partitions based on the regularity that a small fragment of the discontinuity curve appears as a relatively straight ridge as shown in Figure 1a. Such a decomposition strategy is more efficient to represent the 2-D curve or edge than that derived from the wavelet in Figure 1(b).

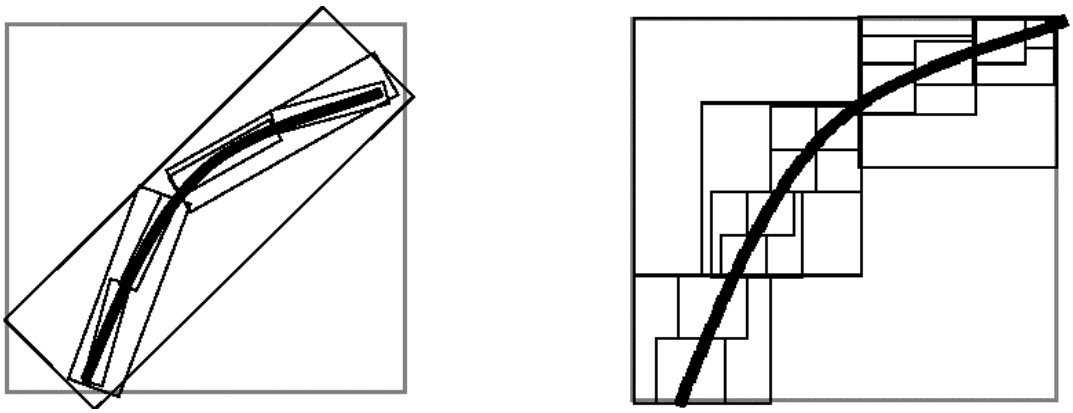

(a) (b)

Figure 1. Subband decomposition of a curve (a) by curvelet transform, and (b) by wavelet transform

(2) Smooth Partitioning

Such subband is further fragmented into square windows w_Q with appropriate size. The high-pass layers $\Delta_s f$ can be multiplied by w_Q to achieve square dissection with the form as $\Delta_s f \to h_Q = (w_Q \cdot \Delta_s f)_{Q \in Q_s}$. The energy of certain pixel $I(x_1, y_1)$ in the image is divided into all sampling grid windows.

(3) Renormalization

The divided squares are renormalized into the unit square [0,1]×[0,1] with the transforming procedure as $g_Q = T_Q^{-1} h_Q$, where T_Q is the normalizing operator.

(4) Ridgelet Transform

A ridge fragment on the renormalized g_Q only needs a very few ridgelet coefficients to represent it as $\alpha_{(Q,\lambda)} = \langle g_Q, \rho_\lambda \rangle$.

3. Regional Entropy Distribution Algorithm

In this section, the fundamental conceptions governing regional entropy and its distribution are proposed for multi-modal medical image fusion.

Based on *à trous* algorithm presented by *Starck* et al. [36], the discrete curvelet transform on medical images can be realized in this article as flow-chart in Figure 2.

Fusion performance is affected by the fusion weight analysis on corresponding coefficients in same decomposing scale of the different source images. The most simple method is to directly average the corresponding coefficients. But as indicated in Figure 1, the curve or edge in its decomposing scale is not just one singular point but has 2-D structure. The regional distribution of coefficients has remarkable influence on the fusion weight of the center coefficient.

For the distribution, one rational method is to measure the *Euclid* distance to the median point in the region, and sets the center coefficient with larger distance to be fused into the corresponding position of the final image. Though such fusion describes how far the local coefficients spread out from the mean point, there has no global sense from the whole scale.

The fusion criterion must be laid on such coefficient that provides the most important information for each local area in the whole domain. In a common sense, edges and curves contain more information than the slowly varying fractions of the image, and the decomposed coefficients corresponding to such curves or edges are also important for offering more information. To discriminate the information amount of coefficient, *Shannon* entropy has been introduced for the masked coefficients regions in curvelet transformed scales.

In viewpoint of information theory, the information entropy is generally expressed in terms of a discrete set of probabilities p_i as

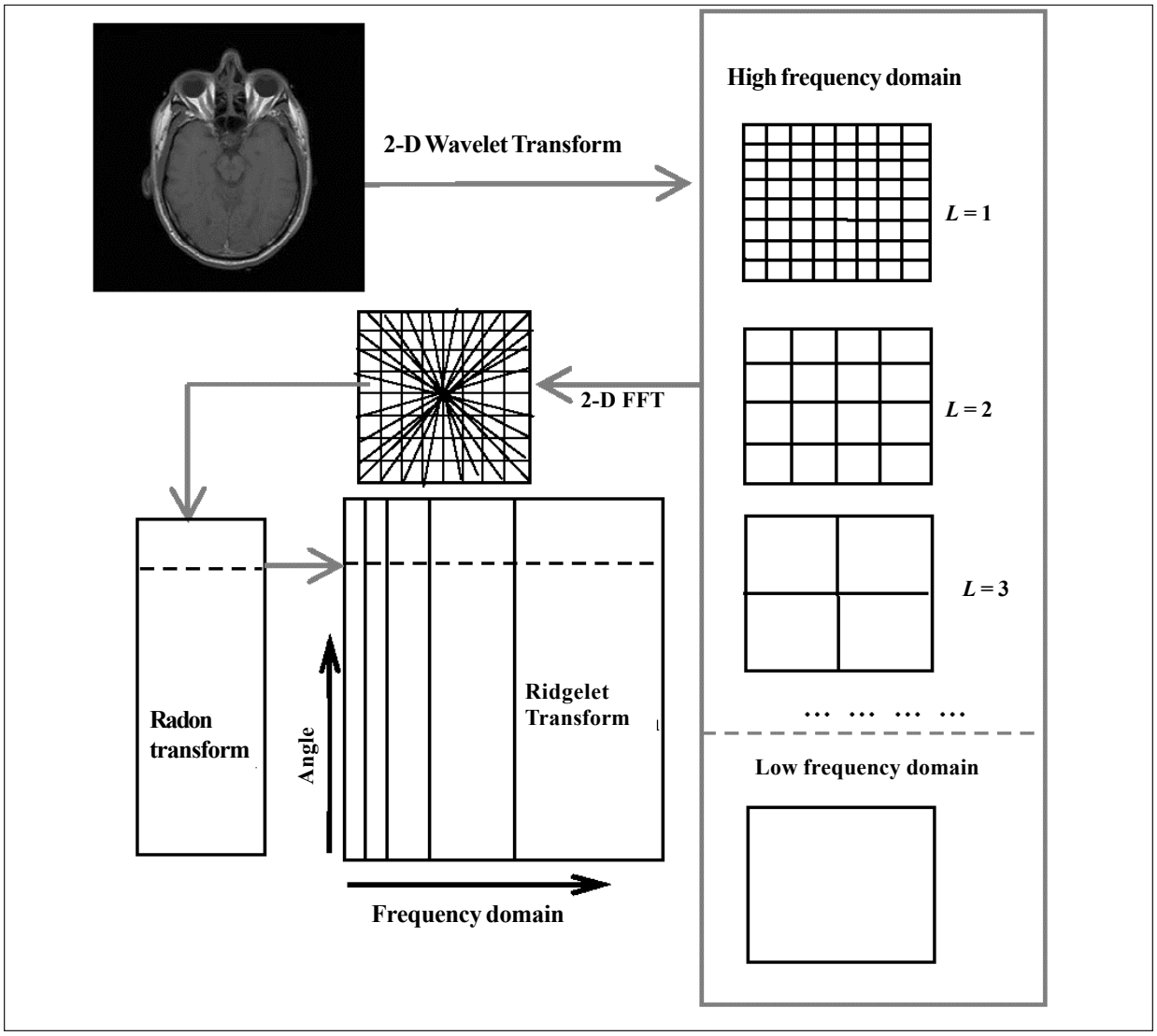

Figure 2. Curvelet transform scheme for 2-D digital medical image exampled by MRI

$$H = -\sum_{i=1}^{n} p_i log_2 p_i \tag{5}$$

In which, p_i is the probability that a particular message is actually transmitted. Entropy H of the message system quantitatively accounts the average amount of information. Such conception is often applied in information content evaluation.

In this article, the entropy concept is generalized for curvelet transformed coefficient information counting in its regional domain.

The curvelet regional entropy distribution rule for counting the fusion weight of the curvelet coefficient can be operated based on the following procedures.

Input: Curvelet transformed coefficient at L-scale as $S_1^J(c_{i,j}), S_2^J(c_{i,j})$ for individual image.

Output: The probability $p_1^L(c_{i,j}), p_2^L(c_{i,j})$, the entropy $H_1^L(c_{i,j}), H_2^L(c_{i,j})$ its regional distribution $\sigma H_1^L(c_{i,j}), \sigma H_2^L(c_{i,j})$, and the fused coefficient $F^L(c_{i,j})$.

Main body:

Procedure 1: { Computing the probabilities from coefficients matrix S_1^L and S_2^L

$$p_1^L(c_{i,j}) = \frac{|S_1^L(c_{i,j})|}{\sum_{i,j}|S_1^L(c_{i,j})|};\ p_2^L(c_{i,j}) = \frac{|S_2^L(c_{i,j})|}{\sum_{i,j}|S_2^L(c_{i,j})|}\ \} \tag{6}$$

Procedure 2 : { Computing the Entropy from Probability Matrix P_1^L and P_2^L. The mask with square form is sliding through all elements of $P_1^L(c_{i,j})$ and $P_2^L(c_{i,j})$.

$$H_1^L(c_{i,j}) = \sum_{i,j}^{mask} p_1^L(c_{i,j})\ log_2\ p_1^L(c_{i,j});\ H_2^L(c_{i,j}) = -\sum_{i,j}^{mask} p_2^L(c_{i,j})\ log_2 p_2^L(c_{i,j})\ \} \tag{7}$$

Procedure 3: { Computing the Entropy Regional Variance from Entropy Matrix H_1^L, H_2^L with sliding windows

$$\begin{aligned} \sigma H_1^L(c_{i,j}) &= \frac{1}{w \times w}\sqrt{\sum_{i,j=1}^{w,w}(H_1^L(c_{i,j}) - \overline{H_1^{L,w}(c_{i,j})})^2}; \\ \sigma H_2^L(c_{i,j}) &= \frac{1}{w \times w}\sqrt{\sum_{i,j=1}^{w,w}(H_2^L(c_{i,j}) - \overline{H_2^{L,w}(c_{i,j})}; \end{aligned} \tag{8}$$

Fusion strategy 1: { $F_p^L(c_{i,j}) = Q_p^L(c_{i,j}) \times S_1^L(c_{i,j}) + (1 - Q_p^L(c_{i,j})) \times S_2^L(c_{i,j})$

$$\text{in which, } Q_p^L(c_{i,j}) = \begin{cases} 1 & p_1^L(c_{i,j}) \geq p_2^L(c_{i,j}) \\ 0 & p_1^L(c_{i,j}) < p_2^L(c_{i,j}) \end{cases}\ \} \tag{9}$$

Fusion strategy 2: { $F_H^L(c_{i,j}) = Q_H^L(c_{i,j}) \times S_1^L(c_{i,j}) + (1 - Q_H^L(c_{i,j})) \times S_2^L(c_{i,j})$

$$\text{in which, } Q_H^L(c_{i,j}) = \begin{cases} 1 & H_1^L(c_{i,j}) \geq H_2^L(c_{i,j}) \\ 0 & H_1^L(c_{i,j}) < H_2^L(c_{i,j}) \end{cases}\ \} \tag{10}$$

Fusion strategy 3: { $F_{\sigma H}^L(c_{i,j}) = Q_{\sigma H}^L(c_{i,j}) \times S_1^L(c_{i,j}) + (1 - Q_{\sigma H}^L(c_{i,j})) \times S_2^L(c_{i,j})$

$$\text{in which, } Q_{\sigma H}^L(c_{i,j}) = \begin{cases} 1 & \sigma H_1^L(c_{i,j}) \geq \sigma H_2^L(c_{i,j}) \\ 0 & \sigma H_1^L(c_{i,j}) < \sigma H_2^L(c_{i,j}) \end{cases}\ \} \tag{11}$$

The fusion strategy based on entropy and its regional distribution is graphically descried in Figure 3.

Above procedures and graphical schemes are programmed in Matlab, and CT/MRI images are selected to illustrate such strategies. CT/MRI images are respectively decomposed into L subbands, and the curvelet decomposed coefficient matrix s^L is corresponding to the coarse or smooth information of the original images. Then each coefficient is manipulated by the above stated regional entropy distribution strategies. Finally, inverse curvelet transform is carried out to reconstruct the fused image. Quantitative parameters such as image entropy, average gradient, standard deviation and mutual information are applied to evaluate the fusion effect.

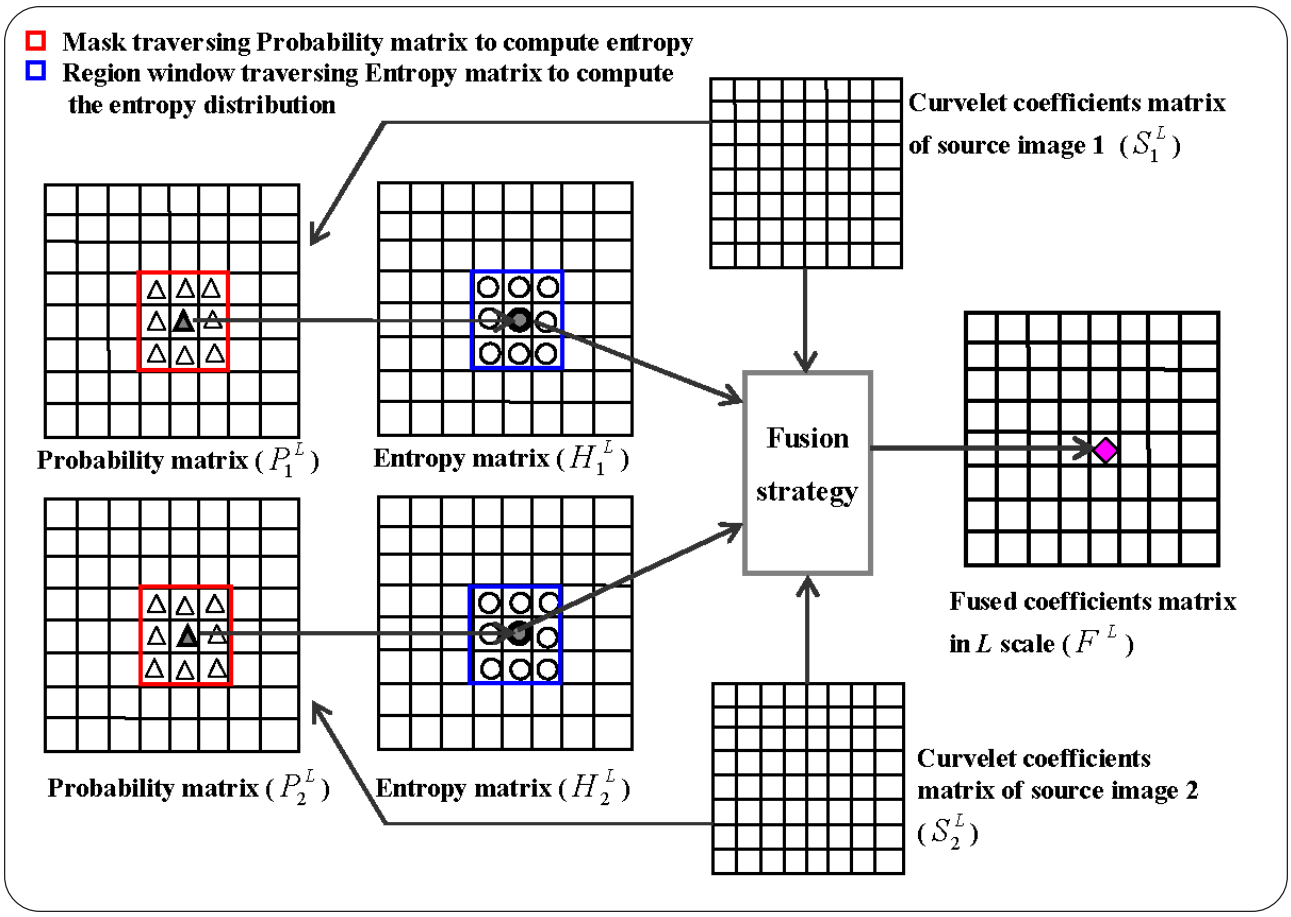

Figure 3. Curvelet regional entropy fusion rule for counting the coefficient fusion weight

4. Results and Discussions

4.1. Preprocessing on the Original Images

The spatially registered original CT and MRI images are show in Figure 4a and 4d, which are sourced from the same man. CT scanning on head is typically used to detect infarction, tumors, hemorrhage, bone trauma and so on. MRI provides good contrast between the soft tissues in the brain. The two imagery methods are complementary to each other, and fusion into a more informative image with surgery significance.

The edge information of original CT and MRI image are outlined in Figure 4b and 4e in order to erase the instrument noise, i.e. the obvious scanning aperture of CT image in Figure 4a. The background denoised CT and MRI images are respectively shown in Figure 4c and Figure 4f, which are further analyzed for their high-resolution features.

The information amount embedded in individual original image is evaluated as image pixel entropy, and calculated according to the following Eq.(12) as

$$H(x) = -\sum_{x=0}^{255} p(x)\, log_2 p(x),\ x = 0, 1, 2, ...255 \tag{12}$$

In which, $p(x)$ is defined as the ratio between the pixel amount with gray level of x and the overall pixel amount in the image. The gray level distribution $p(x)$ is computed based on the following equation and displayed in Figure 5, with $m \times n$ as the image pixel matrix dimension.

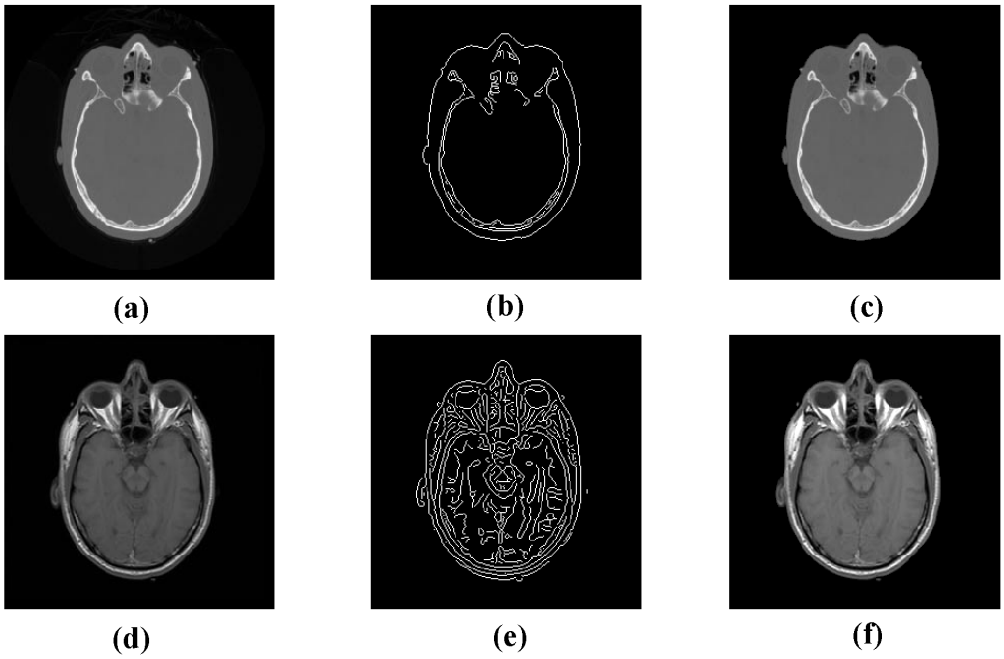

Figure 4. (a), (d) Original CT or MRI image. (b), (e) Edge profile extracted from CT or MRI image. (c), (f) Pre-denoised CT or MRI image based on the edge profiles

$$p(x) = \frac{\sum_{i,j=1}^{m,n} (I(i,j) == x)}{m \times n} \quad \text{(In the selected CT/MRI image, the } m = n = 256.\text{)} \qquad (13)$$

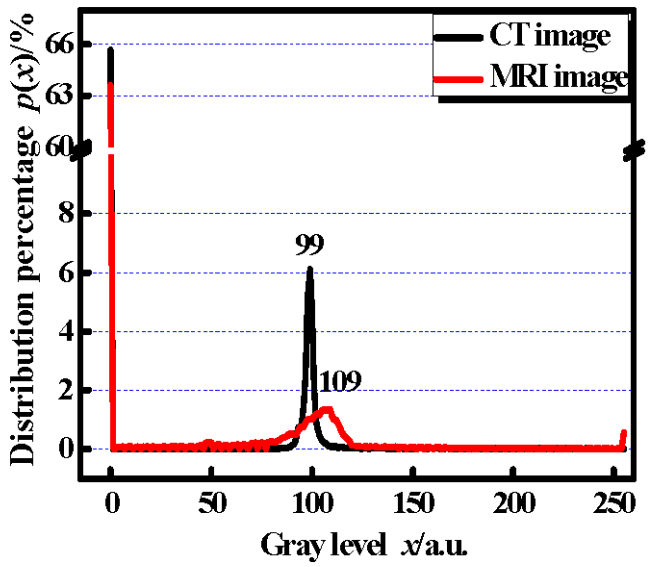

Figure 5. Pixel gray level distribution $p(x)$ of the two original images

It is obvious that the MRI image contains more information than that of CT image due to its wider pixel distribution profile in Figure 5, and the MRI image presents more edges displayed in Figure 4. Such feature is consistent with the computed image entropy as $H_{MRI} = 3.3269$ and $H_{CT} = 2.5856$, respectively.

4.2. Image Fusion based on Curvelet Transform Entropy

The 2-D curvelet transform is applied to the CT and MRI images, respectively. The fused image has been achieved in Figure 6a after algorithm designing and processing based on *Fusion strategy* 1, in which the probabilities $p^L(c_{i,j})$ of curvelet coefficients are acted as fusion criterion. The information embedded in fused image becomes more abundant than each original image, since there has obvious evidence that the CT features have appeared in MRI structures.

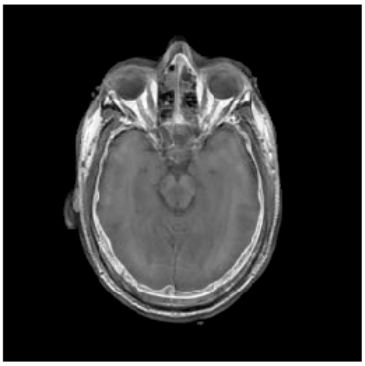

(a)

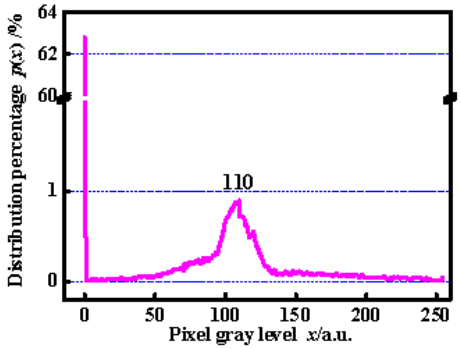

(b)

Figure 6. (a) The fused image based on the proposed Fusion strategy 1. (b) The pixel gray level distribution of the fused image

To calculate the image entropy, pixel gray level distribution $p(x)$ of the fused image is given in Figure 6b. The has considerable wider distribution around pixel gray level of 110, compared to the distribution peaks around 109 of original MRI and around 99 of CT image. The image entropy has increased in a notable extent to 3.6069. The resulted image becomes more informative than any of the original images. Also, it can be seen that more information of MRI has been preserved, and the pixel distribution curve is similar to that of MRI. Since the algorithm is effective to preserve and fuse information sourced from different modal medical images, it is beneficial for diagnosing on brain pathologic change based on the integrated information.

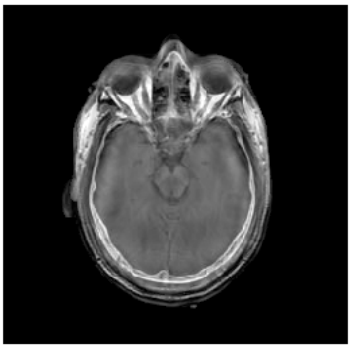

(a)

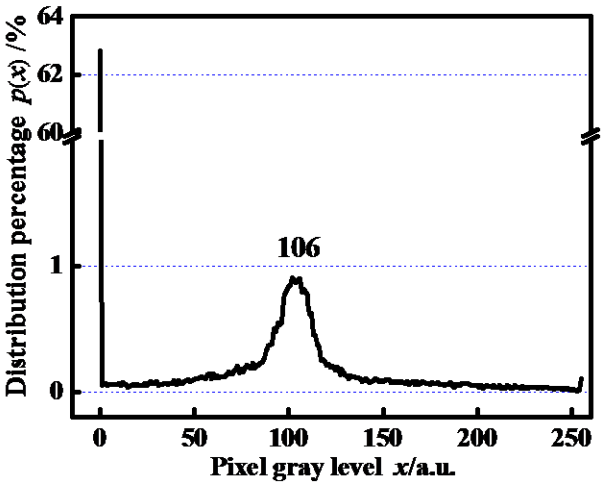

(b)

Figure 7. (a) The fused image based on *Fusion strategy* 2 at 5×5 sized mask manipulated on the Probability matrix. (b) The pixel gray level distribution of the fused image

The *Fusion strategy* 2, which selects the probabilities $P^L(c_{i,j})$ in $w \times w$ sized mask for entropy computation as fusion criteria, has subsequently been processed with the mask designed at 5×5. There has relatively more CT character been preserved than the *Fusion strategy* 1, as shown in figure7a. The peak at 106 appears in the gray level distribution curve in figure 7b, which is moved at left direction to the peak of original CT image around 99.

The image entropy is calculated as 3.6204, which is larger than that in *Fusion strategy* 1 at 0.37% increase extent. Such a result should be ascribed to the reason that the entropy criteria derived from the probability $P^L(c_{i,j})$ matrix at 5×5 sized mask is more sensitive to discriminate the significant coefficients in the curvelet transformation scale. In other words, the 5×5 size masked entropy criterion has discriminated out more CT information than *Fusion strategy* 1.

As a matter of course, the mask size effect on the fusion should be focused on. The mask size of 1×1, namely the direct calculated entropy criteria based on every probability element, has been manipulated. After processing through the above stated procedures, the fusion effect is shown in figure 8a. Its image pixel entropy is 3.6069, which is the same as that of figure 6a based on *Fusion strategy* 1. Such 1×1 sized mask does not contain regional feature for computing entropy fusion weight factor, and the fusion effect is smaller than that based on 5×5 masked entropy criterion.

The other sized masks such as 3×3, 7×7 and 9×9 are also carried out, and the fusion images are respectively present in figure 8b,

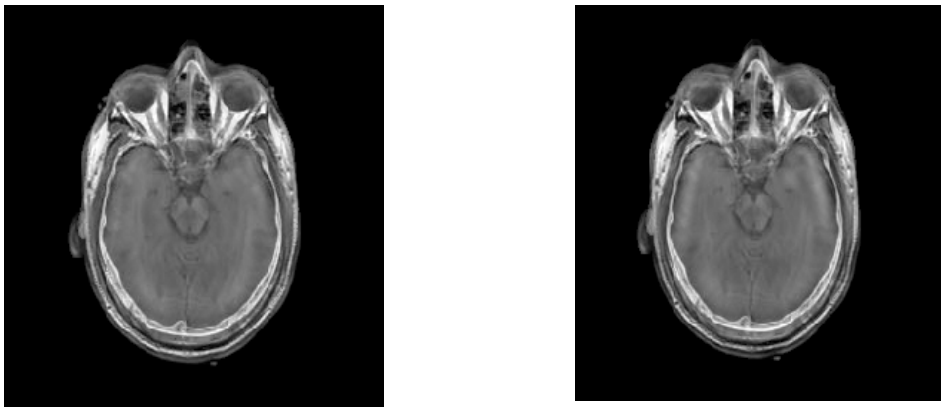

(a) (b)

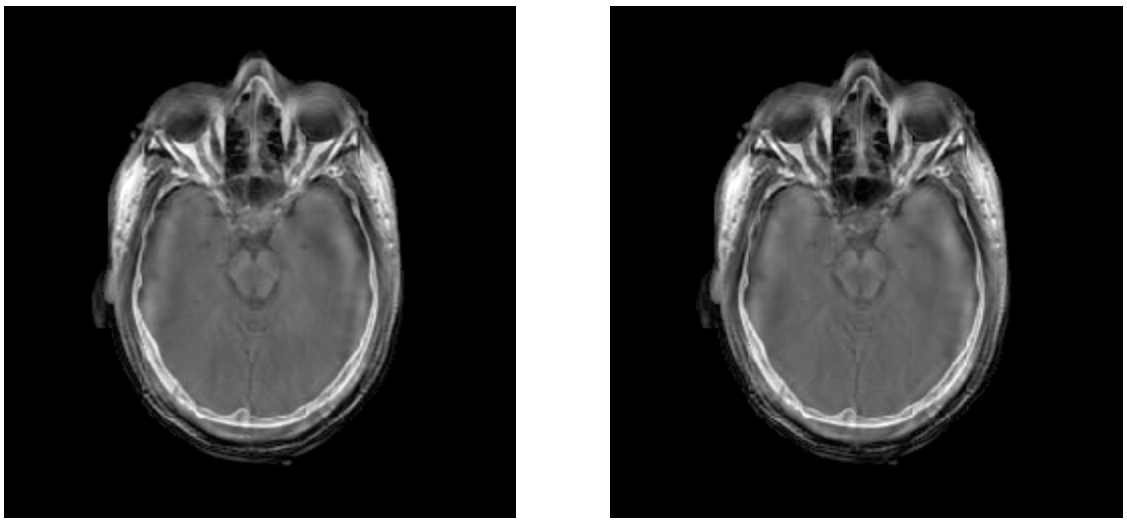

(c) (d)

Figure 8. Image fusion based on *Fusion strategy 2* under entropy weight criteria derived from different sized mask on Probabilities matrix as (a) 1×1, (b) 3×3, (c) 7×7 and (d) 9×9

8c and 8d. It implies in naked eyes observation that the latter two are worse especially at the bottom of the images. For the former 3×3 masked entropy weight criteria, it is obviously prior to 1×1 mask to generate high contrast image. But question is put forward to quantitatively evaluate its fusion effect.

4.3. Evaluation on the Fusion Effects

The rational parameter for image fusion evaluation is the image pixel entropy defined by Eq.(12). The pixel gray level distribution $p(x)$ is shown in Fig. 9a for the five kinds of masked entropy criteria based on *Fusion strategy* 2. It presents that the wider mask can achieve more information extracted from CT image, and the pixel gray level peaks are moved from 106 to 99.

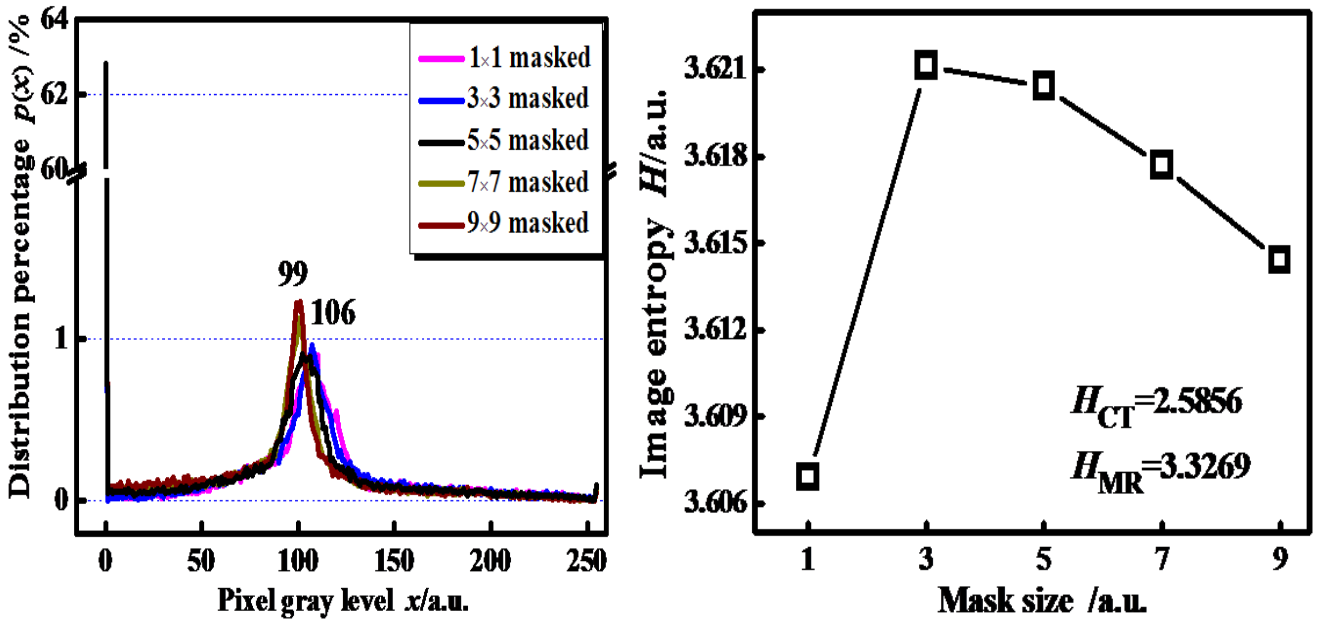

Figure 9. (a) The pixel gray level distribution of the fused images based on different sized mask according to *Fusion strategy* 2. (b) Relationship between the fusion image pixel entropy and the mask size

The fused images possess more information with higher image pixel entropies than the original MRI or CT image as shown in Fig. 9b. The information entropy fused by masks with wider size than 1 is higher than that in *Fusion strategy* 1. It means that *Fusion strategy* 2 is more effective. From all, the mask with size of 3×3 is optimal to achieve more informative.

It also should be noticed that the wider mask is advantageous for extracting CT image information. Such a phenomenon is ascribed that CT image has edges though few in quantities but continuous in profiles as shown in Figure 4b. Wider masks can seek out the curvelet coefficients mapping such CT edges. But the coefficients about short edges mapped from MRI image would be suppressed, as verified by the left-moved gray level distribution peaks.

Fusion effect evaluation parameters are still controversially investigated. Besides the naked-eyes visual observation, the image pixel entropy parameter in Fig. 9 should be combined with the other evaluation methods such as the average gradient, the standard deviation and the mutual information, in order to thoroughly comprehend the fusion effect. To evaluate the performance of the proposed *Fusion strategy* 2, the other evaluation parameters are calculated in Tab. 1 for the original CT and MRI image as well as the 3×3 masked entropy fusion image.

There has remarkable increment of average gradient and standard deviation for the fused image compared to the original images. It means that more details have been fused together. For the mutual information, this parameter presents the communal information between the original images and the fused one. It can be quantitatively deduced that the fused image has more MRI information than CT.

Image / Parameters	CT image	MRI image	Fused image through 3×3 mask
Average gradient ($\overline{G}$)	2.3076	4.3591	4.6527
Standard deviation (σ)	36.3015	37.3765	41.8298
Mutual information (M)	0.8129	1.0016	—

Table 1. Evaluation on original CT and MRI images as well as fused image based on 3×3 masked entropy criteria according to Fusion strategy 2

4.4. Further Fusion based on Regional Entropy Distribution

The Fusion strategy 3 is further applied to the above established 3×3 masked entropy matrix, in order to compute the regional entropy variance. The Fusion strategy 3 resulted images are shown in Figure 10.

Figure 10. (a)-(e): The fused image based on Fusion strategy 3 under 1×1 , 3×3, 5×5, 7×7 and 9×9 sized region to compute the regional entropy variance. (f) The corresponding pixel gray level distribution of fused images in (a)-(e).

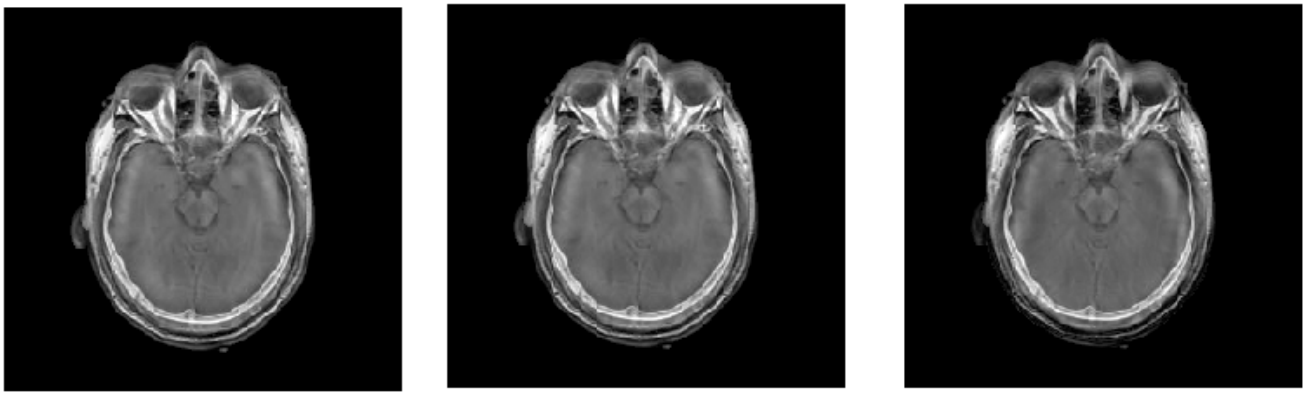

(a) (b) (c)

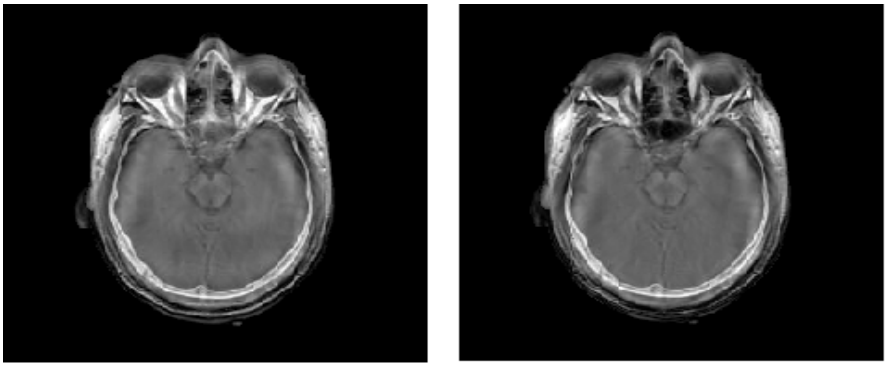

(d) (e)

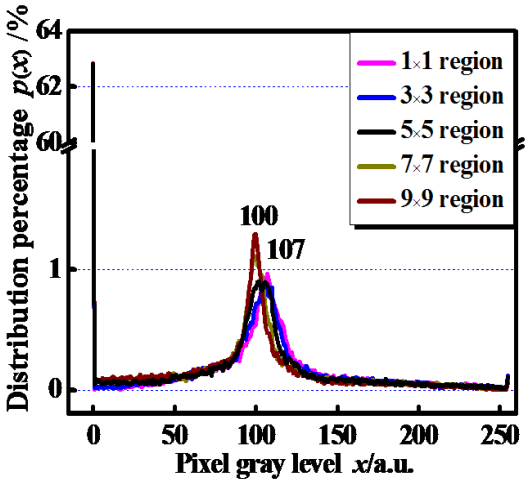

(f)

Figure 10. (a)-(e): The fused image based on *Fusion strategy* 3 under 1×1 , 3×3, 5×5, 7×7 and 9×9 sized region to compute the regional entropy variance. (f) The corresponding pixel gray level distribution of fused images in (a)-(e)

With region width increased, more CT information is also appeared in the fusion images, which is verified by the left moved pixel gray level distribution peaks in Fig.10f. Such a phenomenon is similar to Figure 9a through *Fusion strategy* 2 treatment.

Visual and quantitative image pixel entropy evaluation implies that obvious improvement appeared as shown in Figure 11, especially judged by 3×3 dimension regional entropy variance.

The fusion effect based on such regional entropy variance judgment varies when the region dimension increased. Based on the 3×3 dimension regional entropy variance, the fused image pixel entropy is heightened from 3.6211 to 3.6263, with an increment of 0.14% achieved. The 5×5 region manipulation also obtains improved fusion though with relatively less increment. But the region wider than 5 has deteriorated the image fusion quality. For the 1×1 region, its regional entropy distribution is nonsense, and the same fusion effect is achieved as the *Fusion strategy* 2 based on 3×3 masked entropy criteria.

It can be concluded that wider mask or region is sensitive to CT information, though too wider mask or region would deteriorate the total fusion effect. And the regional entropy distribution criteria from adequate region is more effective to fuse CT and MRI image than only entropy criteria derived from different mask operations.

For comparison, the traditional strategy such as the maximal curvelet coefficient selection rule is also carried out. The operation is directly applied on the curvelet coefficient matrices at each scale. The traditional fusion strategy is described as

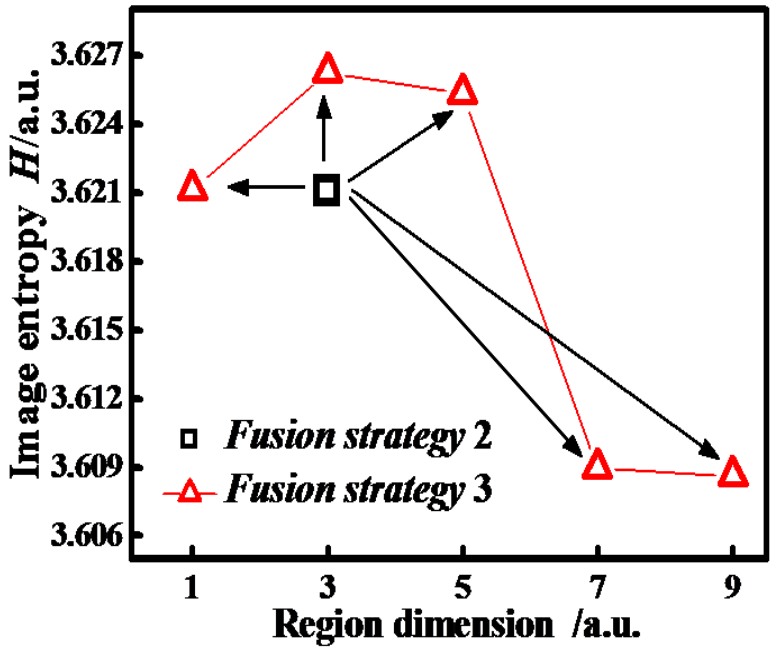

Figure 11. Image pixel entropy of the fused images according to *Fusion strategy* 3 (the triangle symbol “) versus the regional dimension. In this figure, the square symbol (¡%) is the image pixel entropy fused by *Fusion strategy* 2 based on 3×3 masked entropy criteria

Fusion strategy 4: { $F_c^L(c_{i,j}) = Q_c^L(c_{i,j}) \times S_1^L(c_{i,j}) + (1 - Q_c^L(c_{i,j})) \times S_2^L(c_{i,j})$

$$\text{in which, } Q_c^L(c_{i,j}) = \begin{cases} 1 & S_1^L(c_{i,j}) \geq S_2^L(c_{i,j}) \\ 0 & S_1^L(c_{i,j}) < S_2^L(c_{i,j}) \end{cases} \} \quad (14)$$

According to *Fusion strategy* 4, the fusion weight of coefficient $S_1^L(c_{i,j})$ or $S_2^L(c_{i,j})$ in the L^{th} scale is directly decided by the coefficient value. The bigger one is authorized as the essential coefficient with fusion weight of 1, and the smaller is weighted with 0.

As seen in Figure 12, the direct comparison of curvelet coefficients has some effect on multi-modal information fusion, but the contrast of the fused image is relatively poor with break edges appeared in the image. This is not very successful for CT and MRI image fusion.

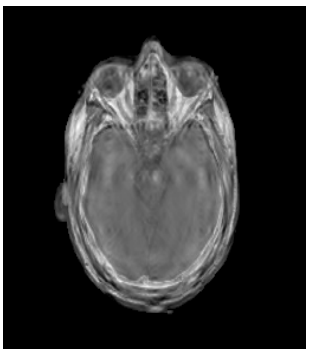

Figure 12. The fused image based on the traditional *Fusion Strategy* 4 through comparing the curvelet coefficient value at corresponding transform scale

Overall, the *Fusion Strategy* 1, 2 and 3 are all prior to the traditional *Fusion Strategy* 4, with *Fusion Strategy* 3 is optimal at the 3×3 regional entropy distribution decision on the 3×3 masked entropy derived from the curvelet coefficient matrices.

5. Conclusion

Combination of different medical images into one image under the premise of spatial registration can often acquire more clinical information than the individual image, i.e. the CT and MRI images can be integrated to determine the profile and structure of tumors or other lesions. In this article, the regional entropy distribution fusion strategy is established based on the curvelet transformation on the individual CT and MRI image.

Results indicate that the curvelet transform entropy criterion is effective to decide the fusion weight. And the 3×3 masked probability matrix can obtain optimal entropy as weight criteria to achieve more effective fusion than the direct comparison of the coefficient probabilities. Fused image embeds higher image pixel entropy than the individual images. The mutual information parameter implies that more MRI information has been fused than that CT.

Further analysis on the regional entropy distribution is applied on image fusion. There has obvious improvement based on the regional entropy variance in 3×3 dimension, and the fused image pixel entropy has been heightened at 0.14% increment extent. The regional entropy distribution criteria are more effective to fuse the CT and MRI image, compared to the only entropy at different masks as fusion weight. When widening the mask size or the region dimension, the proposed strategies are more sensitive to CT image. CT information amount is increased in the fused image, though the total fusion effect is deteriorated.

Consequently, the optimal fusion method based on curvelet transform regional entropy distribution character has been obtained for integrating individual medical images to achieve richer information. More details of the human body tissues can be grasped from the fused image for further clinically analysis.

Acknowledgments

This work is financially supported by the Fundamental Research Funds for the Central Universities No. 2016MS153.

References

[1] Lewis, R.A. (2004). Medical phase contrast X-ray imaging: Current status and future prospects. *Physics in Medicine and Biology* , 49, 3573-3583.

[2] Hendee, W. R. (2003). Ritenour, E.R. *Medical Imaging Physics*. ISBN: 9780471461135, John Wiley & Sons, 2003.

[3] Blake, G. M., Fogelman, I. (2010). An update on dual-energy X-ray absorptiometry. *Seminars in Nuclear Medicine*, 40, 62-73.

[4] Heimann, T., Meinzer, H. P. (2009). Statistical shape models for 3D medical image segmentation: A review. *Medical Image Analysis*, 13, 543-563.

[5] Thibault, J. B., Sauer, K. D., Bouman, C. A., Hsieh, J. (2007). A three-dimensional statistical approach to improved image quality for multislice helical CT. *Medical Physics*, 34, 4526-4544.

[6] Ribeiro, M. X., Traina, C., Azevedo-Marques, P. M. (2008). An association rule-based method to support medical image diagnosis with efficiency. *IEEE Transactions on Multimedia*, 10, 277-285.

[7] Buades, A., Coll, B., Morel, J. M. (2005). A review of image denoising algorithms, with a new one. *Multiscale Modeling & Simulation*, 4, 490-530.

[8] Maintz, J. B., Viergever, M.A. (1998). A survey of medical image registration. *Medical Image Analysis*, 2, 1-36.

[9] Smith, S. M., Jenkinson, M., Woolrich, M. W., Beckmann, C. F., Behrens, T. E. J., Johansen-Berg, H., Bannister, P. R., De Luca, M., Drobnjak, I., Flitney, D. E., Niazy, R. K., Saunders, J., Vickers, J., Zhang, Y. Y., De Stefano, N., Brady, J. M., Matthews, P. M. (2004). Advances in functional and structural MR image analysis and implementation as FSL. *Neuroimage*, 23, S208-S219.

[10] Ma, Z., Tavares, J. M. R., Jorge, R. N., Mascarenhas, T. (2010). A review of algorithms for medical image segmentation and their applications to the female pelvic cavity. *Computer Methods in Biomechanics and Biomedical Engineering*, 13, 235-246.

[11] Mariani, G., Bruselli, L., Kuwert, T., Kim, E.E., Flotats, A., Israel, O., Watanabe, N. (2010). A review on the clinical uses of SPECT/CT. *European Journal of Nuclear Medicine and Molecular Imaging*, 37, 1959-1985.

[12] Kumar, M., Dass, S. (2009). A total variation-based algorithm for pixel-level image fusion. *IEEE Transactions on Image Processing*, 18, 2137-2143.

[13] Yang, L., Guo, B. L., Ni, W. (2008). Multimodality medical image fusion based on multiscale geometric analysis of contourlet transform. *Neurocomputing*, 72, 203-211.

[14] Rahman, M. M., Desai, B. C., Bhattacharya, P. (2008). Medical image retrieval with probabilistic multi-class support vector machine classifiers and adaptive similarity fusion. *Computerized Medical Imaging and Graphics*, 32, 95-108.

[15] Piella, G. (2003). A general framework for multiresolution image fusion: From pixels to regions. *Information Fusion*, 4, 259-280.

[16] Daneshvar, S., Ghassemian, H. (2010). MRI and PET image fusion by combining IHS and retina-inspired models. *Information Fusion*, 11, 114-123.

[17] James, A. P., Dasarathy, B. V. (2004). Medical image fusion: A survey of the state of the art. *Information Fusion*, http://dx.doi.org/10.1016/j.inffus.2013.12.002.

[18] Wang, Z., Ma, Y. (2008). Medical image fusion using m-PCNN. *Information Fusion*, 9, 176-185.

[19] Viceconti, M., Clapworthy, G., Testi, D., Taddei, F., McFarlane, N. (2011). Multimodal fusion of biomedical data at different temporal and dimensional scales. *Computer Methods and Programs in Biomedicine*, 102, 227-237.

[20] Zhao, J., Li, H. Y. (2011). An image fusion algorithm based on multi-resolution decomposition for functional magnetic resonance images. *Neuroscience Letters*, 487, 73-77.

[21] Bhatnagar, G., Jonathan Wu., Q. M., Liu, Z. (2013). Human visual system inspired multi-modal medical image fusion framework. *Expert Systems with Applications*, 40, 1708-1720.

[22] Qu, G. H., Zhang, D. L., Yan, P. F. (2001). Medical image fusion by wavelet transform modulus maxima. *Optics Express*, 9, 184-190.

[23] Shah, P., Merchant, S. N., Desai, U. B. (2013). Multifocus and multispectral image fusion based on pixel significance using multiresolution decomposition. *Signal, Image and Video Processing*, 7, 95-109.

[24] Lewis, J. J., O'Callaghan, R. J., Nikolov, S. G., Bull, D. R. (2007). Canagarajah, N. Pixel-and region-based image fusion with complex wavelets. *Information Fusion*, 8, 119-130.

[25] Singh, R., Khare, A. (2013). Multiscale medical image fusion in wavelet domain. *Scientific World Journal*, 521034.

[26] Singh, R., Srivastava, R., Prakash, O., Khare, A. (2012). Multimodal medical image fusion in dual tree complex wavelet transform domain using maximum and average fusion rules. *Journal of Medical Imaging and Health Informatics*, 2, 168-173.

[27] Yang, Y., Park, D. S., Huang, S. Y., Yang, J. C. (2010). Fusion of CT and MR images using an improved wavelet based method. *Journal of X-Ray Science and Technology*, 18, 157-170.

[28] Kumar, N. S., Shanthi, C. (2007). A survey and analysis of pixel level multisensor medical image fusion using discrete wavelet transform. *IETE Technical Review*, 24, 113-125.

[29] Do, M. N., Vetterli, M. (2005). The contourlet transform: An efficient directional multiresolution image representation. *IEEE Transactions on Image Processing*, 14, 2091-2106.

[30] Candès, E., Demanet, L., Donoho, D., Ying, L. (2008). Fast discrete curvelet transforms. *Multiscale Modeling & Simulation*, 5, 861-899.

[31] Li, S. T., Yang, B. (2008). Multifocus image fusion by combining curvelet and wavelet transform. *Pattern Recognition Letters*, 29, 1295-1301.

[32] Xu, L., Du, J.P., Hu, Q., Li, Q. P. (2013). Feature-based image fusion with a uniform discrete curvelet transform. *International Journal of Advanced Robotic Systems*, 10, 1-10.

[33] Sapkal, R. J., Kulkarni, S. M. (2013). Innovative image fusion algorithm based on fast discrete curvelet transform with different fusion rules. 2013 *IEEE Conference on Information & Communication Technologies* (*ICT*) 2013, 1070-1074.

[34] RRNYI, A. (1961). On measures of entropy and information, *Fourth Berkeley Symposium on Mathematical Statistics and Probability* , 547-561.

[35] Ali, F. E., El-Dokany, I. M., Saad, A. A., Abd El-Samie, F. E. (2010). A curvelet transform approach for the fusion of MR and CT images. *Journal of Modern Optics*, *57*, 273-286.

[36] Starck, J. L., Candès, E. J., Donoho, D. L. (2002). The curvelet transform for image denoising. *IEEE Transactions on Image Processing*, 11, 670-684.